RSC Advances

PAPER

View Article Online
View Journal | View Issue

Cite this: *RSC Adv.*, 2018, **8**, 3889

Schiff base Mn(III) and Co(II) complexes coated on Co nanoparticles: an efficient and recyclable magnetic nanocatalyst for H_2O_2 oxidation of sulfides to sulfoxides

Shokoufeh Ghahri Saremi,*[ab] Hassan Keypour,[a] Mohammad Noroozi [c] and Hojat Veisi [b]

Received 11th October 2017
Accepted 5th January 2018

DOI: 10.1039/c7ra11225d

rsc.li/rsc-advances

In this paper, an effective and selective heterogeneous catalyst was produced by immobilization of manganese and cobalt Schiff base-complexes on Co magnetite nanoparticles (MNP). The catalysts $Co@SiO_2[(EtO)_3Si-L^3]/M$ (M = Mn(III) and Co(II)) were synthesized using $Co@SiO_2$ core–shell nanoparticles and amino-functionalized $Co@SiO_2$. The Schiff base ligand $Co@SiO_2[(EtO)_3Si-L^3]$ was synthesized by reacting $Co@SiO_2$ core–shell nanoparticles with 2-hydroxy 1-naphthaldehyde for the synthesis of $Co@SiO_2[(EtO)_3Si-L^3]/M$. The catalysts were characterized by several techniques, such as FT-IR, TEM, XRD, TGA and VSM. The catalytic activities of the prepared catalysts were studied by oxidation of sulfides to the sulfoxides under different conditions. These catalysts can be easily recovered and reused in at least seven sequential cycles without considerable leaching and loss of reactivity.

Introduction

Since the oxidation reactions have potential for generating a wide range of drugs and fine chemicals, they are very important to the chemical industry. Conventionally, oxidation reactions have been carried out using environmentally unfavorable reagents, solvents and catalysts. Hence, efforts have been made towards the development of efficient, easily recoverable, highly selective and reusable heterogeneous catalysts. Recently magnetic nanomaterials have attracted significant attention in oxidation reactions because of their catalytic activity and easy separation.[1–5]

Schiff base transition metal complexes as catalysts have been widely used because of their potential use in numerous reactions,[6,7] such as hydrogenation of organic substrates,[8] epoxidation of olefins,[9] conversion of epoxides into halohydrines,[10,11] asymmetric ring opening of terminal epoxides[12] and oxidation reactions.[13–15] In recent years some publications have been reported sulfides-oxidation using phthalazine-based di-iron complexes,[16] β-brominated *meso*-tetraphenylporphyrinato manganese(III) acetate,[17] copper Schiff base complex,[18] immobilized metalloporphyrins,[19] TsOH by phenyliodine diacetate as an oxidant,[20] dendritic bis(acylamino) pyridines,[21] Schiff base of Mn(III) complex supported on magnetic cobalt nanoparticles,[22] Schiff base complexes of Ni, Co, Cr, Cd and Zn supported on Fe_3O_4 magnetic nanoparticles,[23] magnetic nanoparticle immobilized *N*-propylsulfamic acid,[24] Au/CTN–silica catalyst,[25] cobalt(II), copper(II), zinc(II) and palladium(II) Schiff base complexes,[26] 1,4-bis(3-methylimidazolium-1-yl) butane ditribromide,[27] carboxylated multi-walled carbon nano tubes,[28] 1,4-bis(3-methylimidazolium-1-yl) butane ditribromide $[bMImB](Br_3)_2$ ionic liquid reagent[29] and Mo(VI) complex supported on Fe_3O_4 nanoparticles.[30] In this study, new heterogeneous nanocatalysts were synthesized by chemical modification of surface magnetic nanoparticles of Co with Schiff-base ligands, followed by complex formation through the reaction with Co(II) and Mn(III) salts. Furthermore, the catalytic behavior of these complexes was investigated by carrying out the oxidation of sulfides to sulfoxides under mild conditions.

Experimental

Materials and equipments

All solvents used in this study such as THF, C_2H_5OH, DMSO, DMF, CH_2Cl_2, ethyl acetate, MeOH, $CHCl_3$, acetone, and MeCN (analytical grade) were purchased from Fluka or Merck and used without further purification. In addition, cobalt chloride hexahydrate, citric acid, sodium borohydride, 3-aminopropyltriethoxysilane (APTES), tetraethoxysilane (TEOS), 2-hydroxy 1-naphthaldehyde, Mn $(acac)_3$, H_2O_2 (analytical grade 30% aqueous solution), and $Co(CH_3COO)_2$ were purchased from Fluka or Merck. HPLC grade methyl phenyl sulfide and other

[a]Faculty of Chemistry, Bu-Ali Sina University, Hamedan 65174, Iran
[b]Department of Chemistry, Payame Noor University, Tehran, Iran. E-mail: sho.saremi@gmail.com
[c]Center for Research and Development of Petroleum Technologies at Kermanshah, Research Institute of Petroleum Industry (RIPI), Iran

sulfide compounds were purchased from Aldrich in order to test the performance of the catalysts.

Nanocatalysts were characterized using a Holland Philips PW-1840 with monochromatic Cu Kα radiation and λ 1.54 Å X-ray powder diffraction (XRD) diffractometer at a scanning speed of 2° min^{-1} from 5° to 80° (2θ). The particle size and morphology were investigated using scanning electron microscopy (SEM) (Holland Philips XL30 microscope) at an accelerating voltage of 25 kV. The FT-IR measurements (4000–400 cm^{-1}) were performed using KBr disc on a Shimadzu Fourier Transform Infrared spectra (FT-IR) 8400. The ^{1}H- and ^{13}C-spectra were recorded at 90 MHz, on a Bruker DRX 500-Avance FT NMR instrument with $CDCl_3$ as the solvent. Elemental analysis for C, H and N were performed using a Perkin-Elmer 2400 series analyzer. Thermogravimetric Analysis (TGA) was performed on a Mettler Toledo TGA SDTA 85-e instrument at 30–800 °C with a temperature gradient of 10 °C min^{-1}.

Preparation of the magnetic Co@SiO_2–NH_2 amine (3). The overall synthesis process of the nanocatalyst Co@SiO_2[$(EtO)_3$-Si–L^3]/M (M = Co(II) and Mn(III)) (**6**) is shown in Scheme 1. Magnetic Co@SiO_2–NH_2 amine was synthesized according to the procedure previously reported in literature.[15] First, to a solution of 1 g cobalt chloride hexahydrate in 60 mL distilled water, 0.07 g of citric acid was added and the solution was stirred for 2 min under nitrogen atmosphere. Then, a solution of 3 g sodium borohydride in 100 mL distilled water was added dropwise to the stock solution under nitrogen atmosphere. During the addition of $NaBH_4$, cobalt nanoparticles were formed and the color of the solution changed to black. The nanoparticles were first stabilized by the addition of citrate. After reduction, the particles remained stable for several hours. A perfect monomer formation is generally favored through decreased concentration of cobalt nuclei and good long-time dispersion after citrate stabilization to ensure that the core particles are well separated before coating begins.

Second, the cobalt magnetic core was coated with the SiO_2 shell to obtain core–shell nanoparticles Co@SiO_2. The solution containing Co nanoparticles was stirred for 30 min. Then, under nitrogen atmosphere, 200 μL ethanolic solution of 3-aminopropyl-triethoxysilane (APTES) and 800 μL tetraethoxysilane (TEOS) was sequentially added to the solution. The nitrogen atmosphere was discontinued and the resultant solution was vigorously stirred for 24 h. Finally, the obtained black precipitate was collected with an external magnet, washed twice with deionized water and ethanol and dried at 50 °C in the oven.

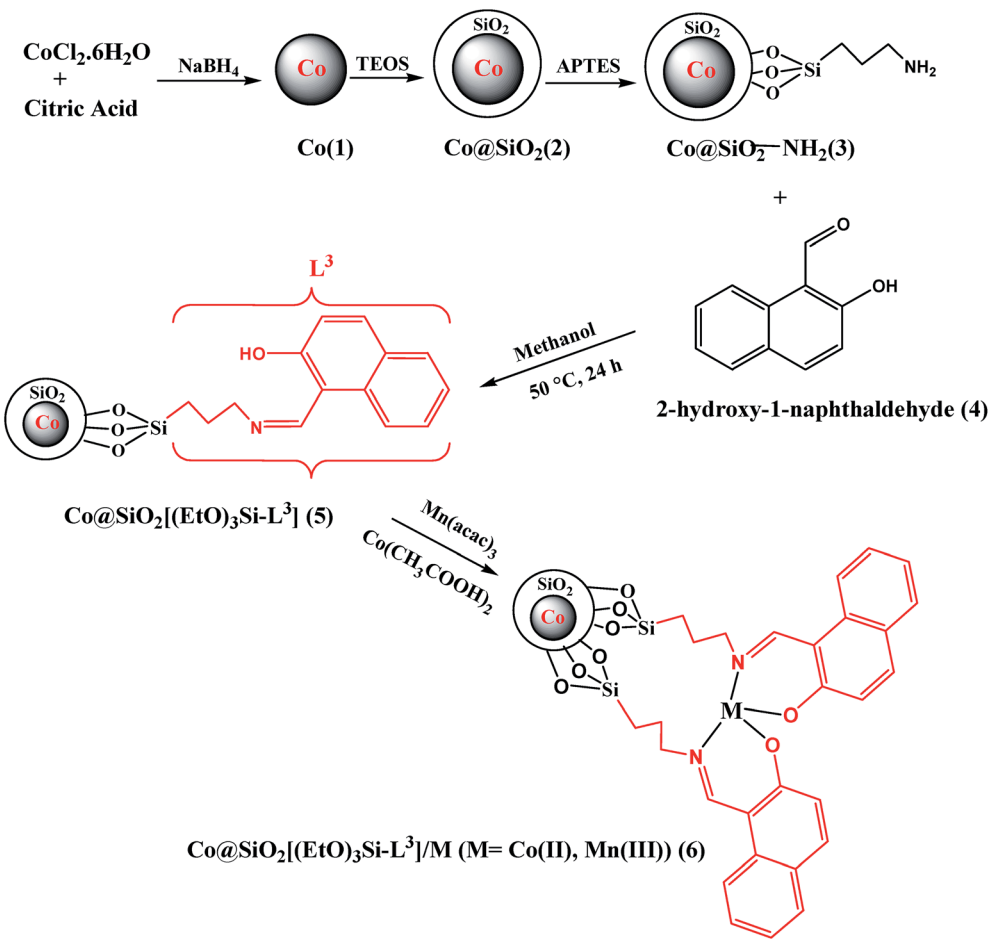

Scheme 1 Preparation of Co@SiO_2[$(EtO)_3$Si–L^3]/M (M = Mn(III) and Co(II)) nanocatalysts.

Further, 3.0 g of the resultant $Co@SiO_2$ was dispersed in 150 mL toluene for 50 min *via* sonication. Then, 11.25 mL (48.06 mmol) of APTES was added dropwise to the mixture with vigorous mechanical stirring. The mixture was refluxed for 15 h. Eventually, the reaction mixture was cooled and the resultant precipitate was collected with an external magnet, washed twice with deionized water and ethanol and the dried at 55 °C in the oven.

Preparation of $Co@SiO_2[(EtO)_3Si–L^3]$ (5). For the preparation of the Schiff base ligand (**5**), the obtained amine in the previous step was reacted with the 2-hydroxy-1-naphthaldehyde.

First, 1.0 g of $Co@SiO_2–NH_2$ was dispersed in 60 mL of dry methanol by sonication for 20 min. Then, 1.20 g (7 mmol) of 2-hydroxy 1-naphthaldehyde was added to the mixture. After stirring at 50 °C for 24 h, the reaction flask was left undisturbed to be cooled. Then, the obtained precipitate was collected with an external magnet and washed twice with dry methanol and dried under vacuum for 20 h.

Preparation of $Co@SiO_2[(EtO)_3Si–L^3]$/M (M = Co(II) and Mn(III)) (6). Initially, 300 mg of $Co@SiO_2[(EtO)_3Si–L^3]$ was ultrasonically dispersed in 30 mL ethanol for 30 min. Then, Mn $(acac)_3$ (1 mmol) was dissolved in 10 mL ethanol. This solution was added to the dispersion of $Co@SiO_2[(EtO)_3Si–L^3]$. The mixture was refluxed for 10 h. Then, the $Co@SiO_2[(EtO)_3Si–L^3]$/Mn(III) was isolated by an external magnet and washed with ethanol, water and acetone, in sequence. All the above steps were also performed for the preparation of $Co@SiO_2[(EtO)_3Si–L^3]$/Co with $Co(CH_3COO)_2$ instead of Mn $(acac)_3$.

The Mn content in $Co@SiO_2[(EtO)_3Si–L^3]$/Mn(III) catalyst was determined to be 4.41 wt% by atomic absorption spectroscopic (AAS) analysis. The percent cobalt in the $Co@SiO_2[(EtO)_3Si–L^2]$/Co(II) was determined to be 12.43 wt%. This value is attributed to the cobalt magnetic core and metal in the complex. The prepared catalysts were characterized by FT-IR, XRD, FESEM, EDX, TEM, and VSM.

General procedure for oxidation of sulfides to sulfoxides. In a typical reaction, a 25 mL reaction flask was charged with 0.02 g of the catalyst $Co@SiO_2[(EtO)_3Si–L^3]$/M, 1 mmol of the methyl phenyl sulfide, 3 mL of ethyl acetate and 60 μL H_2O_2 (30%). The reaction mixture was stirred at 50 °C. The progress of reaction was monitored by thin layer chromatography (TLC).

Results and discussion

Characterization of the catalysts

Fig. 1 shows the FT-IR absorption spectrum of $Co@SiO_2–NH_2$ (a), $Co@SiO_2[(EtO)_3Si–L^3]$ (b), $Co@SiO_2[(EtO)_3Si–L^3]$/Mn(III) (c), and $Co@SiO_2[(EtO)_3Si–L^3]$/Co(II) (d). The FT-IR spectrum for pure $Co@SiO_2–NH_2$ (curve a)[15] shows a stretching vibration at 3445 and 1627 cm^{-1} that are characteristic of symmetrical and asymmetrical modes of the O–H bonds on the surface cobalt nanoparticles, respectively. The peaks at 2901 and 2872 cm^{-1} are assigned to the methylene (–CH_2) of the propyl group, respectively, which indicates that APTES molecules were attached to the surface of the silica-coated MNPs. The main

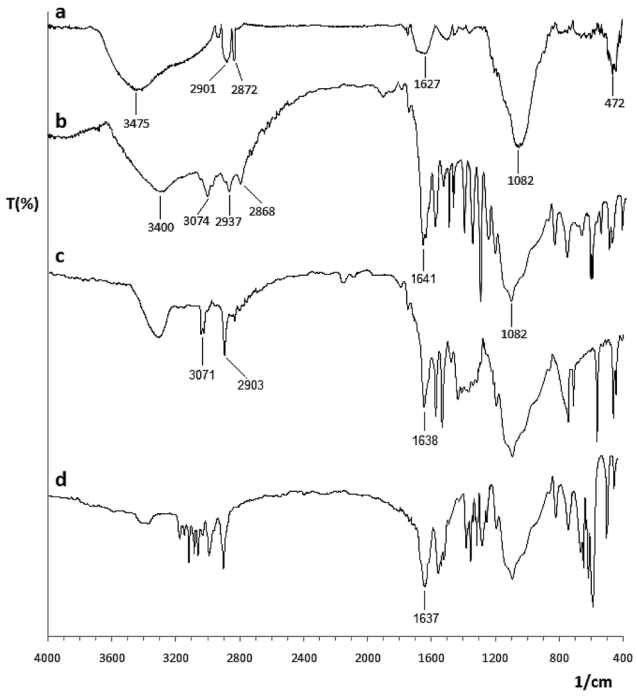

Fig. 1 FT-IR spectra of (a) $Co@SiO_2–NH_2$, (b) $Co@SiO_2[(EtO)_3Si–L^3]$, (c) $Co@SiO_2[(EtO)_3Si–L^3]$/Mn(III) and (d) $Co@SiO_2[(EtO)_3Si–L^3]$/Co(II).

peak at 1082 cm^{-1} indicates the formation of silica layer on magnetic cobalt NPs.

In the FT-IR spectrum of 2-hydroxy-1-naphthaldehyde, a band appears at 1652 cm^{-1}, which is assigned to (C=O) vibration of carbonyl group. In the FT-IR spectrum of $Co@SiO_2[(EtO)_3Si–L^3]$ (curve b), this band was shifted to 1641 cm^{-1} (lower wavenumber), which is attributed to the formation of the imine bond (C=N) on the surface of the magnetic cobalt NPs. Vibrations in the range of 1480–1600 cm^{-1} can be assigned to the aromatic ring.

The IR spectrum of $Co@SiO_2[(EtO)_3Si–L^3]$/Mn(III) complex (curve c) shows a vibrational peak at 1638 cm^{-1}, corresponding to (C=N) bond. The shift in stretching vibration to lower frequency in the complex in comparison to free ligand (1641 cm^{-1}) indicates the formation of metal–ligand bonds. This band in the complex $Co@SiO_2[(EtO)_3Si–L^3]$/Co(II) (curve d) appears at 1637 cm^{-1}. From the comparison between these spectra, it can be concluded that first, the reaction for the formation of an imine has occurred, and second, the reaction for the formation of the complex occurred at the surface of the nanoparticles.

Fig. 2 illustrates the TGA curves, showing the mass loss of the samples as they decompose upon heating. The heating rate is 10 °C min^{-1} between 30 and 800 °C. The metal ions (cobalt, manganese and silicone) and organic materials of the samples were completely converted into metals, metal oxides and burn to generate gaseous products at elevated temperatures. The first mass loss in the thermal analysis of $Co@SiO_2$ (curve a) is observed in the temperature range 90–250 °C (4.35%) due to removal water molecules present at the surface

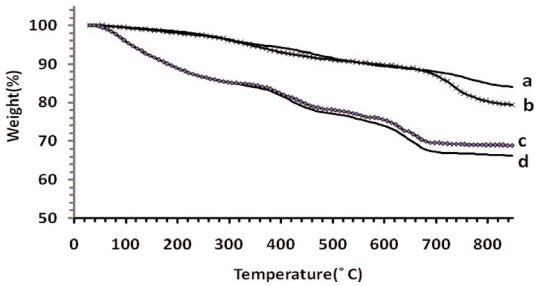

Fig. 2 TGA spectra of (a) $Co@SiO_2$, (b) $Co@SiO_2–NH_2$ (c) $Co@SiO_2[(EtO)_3Si–L^3]/Co(II)$ and (d) $Mn@SiO_2[(EtO)_3Si–L^3]/Co(III)$.

of nano cobalt. The second small weight loss (5.52%) occurred in the region of 280–480 °C, which is related to the removal of trapped water molecules from the lattice. The subsequent weight loss (5.16%) appears in the range of 500–750 °C that is related to the decomposition of SiO_2. In the TGA curve of $Co@SiO_2–NH_2$ (curve b), the small weight loss is observed in the range of 40–150 °C (1.10%) and 150–280 °C (3.55%), which is assigned to the physical loss of the adsorbed or trapped lattice water, respectively. A weight loss is detected in the range of 300–450 °C and 500–750 °C, which are predominantly attributed to the decomposition of organic substances in magnetic Co nanoparticles.[15] The loss in mass for $Co@SiO_2[(EtO)_3Si–L^3]/Co(II)$ and $Co@SiO_2[(EtO)_3Si–L^3]/Mn(III)$ catalysts according to curves c and d is 31.17% and 33.77%, respectively. These results are related to the loss of $[(EtO)_3Si–L^3]$ coated on the Co nanoparticles in the complexes and prove the attachment of $[(EtO)_3Si–L^3H]$ moiety on to the surface of Co nanoparticle.

Therefore, the results of the TG curves correspond to the results of the infrared spectra, which indicate that the surface of the nanoparticles is covered with the ligand functional groups.

As shown in Fig. 3 (curve a and b), for core magnetic cobalt NPs, diffraction peaks with 2θ at 44.2°, 51.5° and 75.9° correspond to (111), (200) and (220) Braggs reflection, respectively indicative of an fcc metallic cobalt structure of the magnetite (card 15-0806 in the JCPDS file). The XRD patterns of $Co@SiO_2[(EtO)_3Si–L^3]/Mn(III)$ and $Co@SiO_2[(EtO)_3Si–L^3]/Co(II)$ show a visible diffusion peak at 2θ = 15–25° that appeared because of the existence of amorphous silica. XRD pattern of $Co@SiO_2$ $[(EtO)_3Si–L^3]/Mn(III)$ complex (curve a) shows three major peaks in the range of 20–40°. XRD pattern of $Co@SiO_2[(EtO)_3Si–L^3]/Co(II)$ (curve b) can be assigned to the diffraction from the three major peaks with 2θ at 19°, 30° and 40° reflection indexes of (100), (200) and (220) planes, respectively (card 25-0250 in the JCPDS file).[15]

Fig. 4 shows the TEM images of $Co@SiO_2[(EtO)_3Si–L^3]/Mn(III)$ (a) and $Co@SiO_2[(EtO)_3Si–L^3]/Co(II)$ (b). As observed from the images, the Schiff base complex Mn(III) and Schiff base complex Co(II) shell (black color) were surrounded by the Co nanoparticles (ash color) and core–shell-type supports were obtained. This indicates the successful coating on the surface of the magnetic nanoparticles. It can be observed that the size of Co nanoparticles is in range of 20–30 nm.

As shown in Fig. 5, the morphology of the $Co@SiO_2[(EtO)_3Si–L^3]/Mn(III)$ and $Co@SiO_2[(EtO)_3Si–L^3]/Co(II)$ was evaluated using scanning electron microscopy. SEM images Fig. 5a and b indicate that the catalysts were composed of nanometer-sized particles. It can be observed that the particles are not fully spherical. In addition, some particle aggregations are observed, which are likely to be caused by the magneto static interactions between particles.

To investigate the catalyst composition, $Co@SiO_2[(EtO)_3Si–L^3]/Mn(III)$ and $Co@SiO_2[(EtO)_3Si–L^3]/Co(II)$ were analyzed using energy dispersive X-ray spectroscopy (EDX) (Fig. 6). The EDX spectrum of $Co@SiO_2[(EtO)_3Si–L^3]/Co(II)$ showed the presence of Si, Co, C, O, and N atoms (curve b). In the EDX spectrum of $Co@SiO_2[(EtO)_3Si–L^3]/Mn(III)$, in addition to the mentioned atoms, the signals of manganese is also seen (curve a). These results once again confirm that the nanoparticles are completely covered with functional groups containing nitrogen, oxygen, *etc.*

Magnetic characterization of the $Co@SiO_2[(EtO)_3Si–L^3]/Mn(III)$ and $Co@SiO_2[(EtO)_3Si–L^3]/Co(II)$ was performed using a vibrating sample magnetometer (VSM). Plots of magnetization *versus* magnetic field at 300 K for the two catalysts are shown in Fig. 7. As shown in the figure, the plots of the catalysts indicate a superparamagnetic behavior. The measured saturation magnetization value (36.28 emu g^{-1} for $Co@SiO_2[(EtO)_3Si–L^3]/Mn(III)$ and 35.98 emu g^{-1} for $Co@SiO_2[(EtO)_3Si–L^3]/Co(II)$)

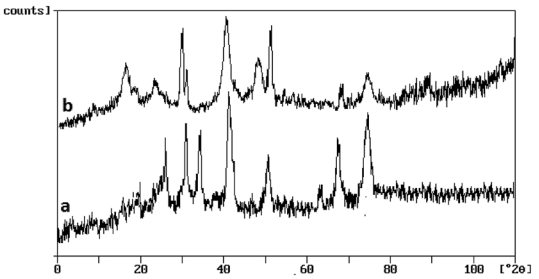

Fig. 3 The X-ray diffraction patterns of (a) $Co@SiO_2[(EtO)_3Si–L^2]/Mn(III)$ and (b) $Co@SiO_2[(EtO)_3Si–L^2]/Co(II)$.

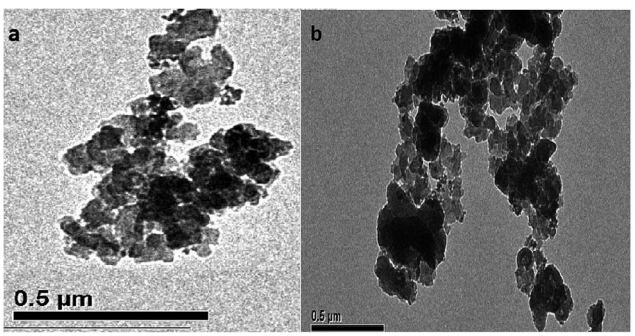

Fig. 4 TEM image of (a) $Co@SiO_2[(EtO)_3Si–L^3]/Mn(III)$ and (b) $Co@SiO_2[(EtO)_3Si–L^3]/Co(II)$.

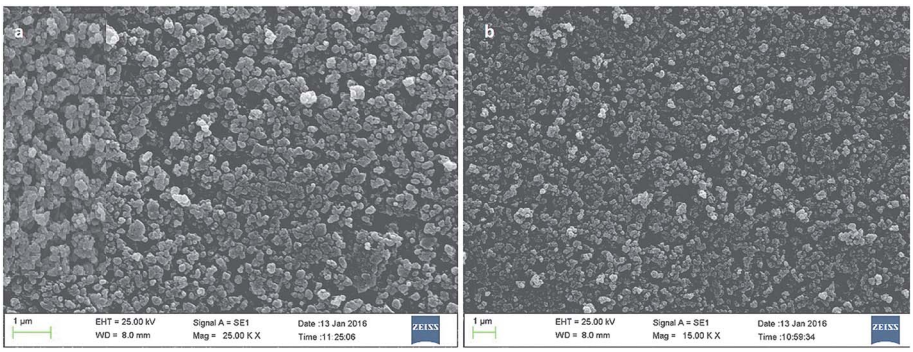

Fig. 5 SEM image of (a) Co@SiO_2[$(EtO)_3Si–L^3$]/Mn(III) and (b) Co@SiO_2[$(EtO)_3Si–L^3$]/Co(II).

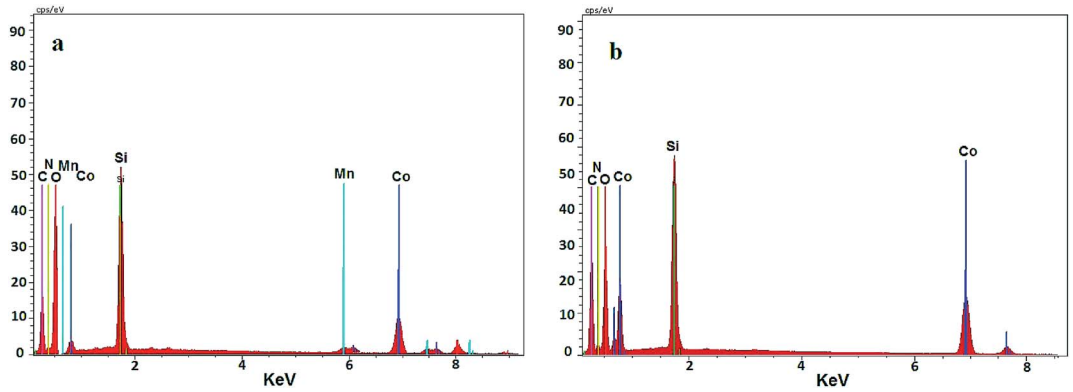

Fig. 6 Energy-dispersive X-ray spectroscopy (EDX) of (a) Co@SiO_2[$(EtO)_3Si–L^3$]/Mn(III) and (b) Co@SiO_2[$(EtO)_3Si–L^3$]/Co(II).

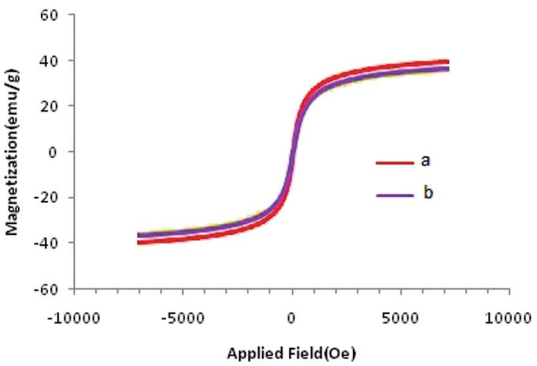

Fig. 7 Room temperature magnetization curves of (a) Co@SiO_2[$(EtO)_3Si–L^3$]/Mn(III) and (b) Co@SiO_2[$(EtO)_3Si–L^3$]/Co(II).

demonstrate smaller saturation magnetization values of the bare Co nanoparticles (39.78 emu g^{-1}).[15] This could be due to SiO_2[$(EtO)_3Si–L^3$] coating on the surface of Co NPs. Nevertheless, their magnetization is sufficient and these magnetic nanoparticles can be quickly separated from their dispersion by using an external magnetic field.

The complexes of Co@SiO_2[$(EtO)_3Si–L^3$]/Mn(III) and Co@SiO_2[$(EtO)_3Si–L^3$]/Co(II) were analyzed by a Perkin-Elmer 2400 series analyzer and elemental analysis results showed a significant C, H, and N content. Anal. found for Co@SiO_2[$(EtO)_3Si–L^3$]/Mn(III): C, 21.53; H, 1.70; N, 2.01 and for Co@SiO_2[$(EtO)_3Si–L^3$]/Co(II): C, 22.08; H, 1.74; N, 2.11. The calculated percentage of elemental analysis for ligand L^3 is: C, 71.00; H, 6.36; N, 5.52. After analyzing these results, it can be concluded that the ratio of the percentage of the elements in the two complexes corresponds to the ratio of these elements in the ligand L^3.

Catalytic activities of the synthesized catalysts

The catalytic activity of Co@SiO_2[$(EtO)_3Si–L^3$]/M (M = Mn(III), Co(II)) was examined through the oxidation of sulfides to sulfoxides (Scheme 2).

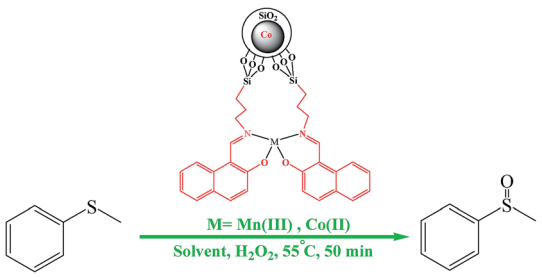

Scheme 2 Co@SiO_2[$(EtO)_3Si–L^3$]/M (M = Mn(III), Co(II)) catalysts for oxidation of sulfide.

First, the oxidation reaction of the methyl phenyl sulfide to methyl phenyl sulfoxide was selected as the model reaction. The catalysts were tested under the following reaction conditions: methyl phenyl sulfide (0.5 mmol), hydrogen peroxide 30% (90 μL, 0.881 mmol), catalyst 0.02 g, reaction time 50 min, reaction temperature 50 °C and various solvents without optimized amounts. The results are summarized in Table 1. As indicated by the data, the catalysts are highly active and selective. In addition, it can be seen that excellent yield of product was obtained in acetonitrile. To determine the reaction yield, the following procedure was adopted. After completion of reaction and separation of catalyst using a magnet, the organic phase was extracted with ethanol. Then, it was dried over sodium sulfate and evaporated. In the next step, the obtained product was recrystallized with ethanol. The resultant sulfoxide was weighed and the reaction yield was calculated. In order to analyze the products formed during the reaction, FT-IR technique was used. FT-IR analysis of the obtained product from the oxidation of sulfide compounds shows S=O stretching frequency at 1049 cm^{-1}, indicating the formation of sulfoxide from sulfide. There is a band at 692 cm^{-1}, corresponding to C–S stretching frequency. Since there is no stretching frequency band observed at 1150 cm^{-1}, corresponding to sulfone, we understand that sulfide is not oxidized to sulfone under the present experimental conditions. The product analysis study demonstrates that sulfoxide is the only product formed under the present reaction conditions.

The effect of temperature was investigated by carrying out the model reaction at different temperatures in acetonitrile. As shown in Fig. 8a, the best result was achieved at 65 °C. Furthermore, the different reaction times were examined at

Table 1 Catalytic results oxidation of methyl phenyl sulfide to methyl phenyl sulfoxide with H_2O_2 by various catalysts and different solvents[a]

Entry	Catalyst	Solvent	Selectivity (%)	Isolated yield
1	$Co@SiO_2[(EtO)_3Si–L^3]/Mn(III)$	THF	100	52
2	$Co@SiO_2[(EtO)_3Si–L^3]/Mn(III)$	C_2H_5OH	100	77
3	$Co@SiO_2[(EtO)_3Si–L^3]/Mn(III)$	DMSO	100	45
4	$Co@SiO_2[(EtO)_3Si–L^3]/Mn(III)$	DMF	100	84
5	$Co@SiO_2[(EtO)_3Si–L^3]/Mn(III)$	CH_2Cl_2	100	49
6	$Co@SiO_2[(EtO)_3Si–L^3]/Mn(III)$	Ethyl acetate	100	69
7	$Co@SiO_2[(EtO)_3Si–L^3]/Mn(III)$	$CHCl_3$	100	73
8	$Co@SiO_2[(EtO)_3Si–L^3]/Mn(III)$	Acetone	100	77
9	$Co@SiO_2[(EtO)_3Si–L^3]/Mn(III)$	MeCN	100	89
10	$Co@SiO_2[(EtO)_3Si–L^3]/Mn(III)$	CH_3OH	100	84
11	$Co@SiO_2[(EtO)_3Si–L^3]/Co(II)$	THF	100	41
12	$Co@SiO_2[(EtO)_3Si–L^3]/Co(II)$	MeCN	100	72
13	$Co@SiO_2[(EtO)_3Si–L^3]/Co(II)$	DMSO	100	35
14	$Co@SiO_2[(EtO)_3Si–L^3]/Co(II)$	C_2H_5OH	100	82
15	$Co@SiO_2[(EtO)_3Si–L^3]/Co(II)$	CH_2Cl_2	100	48
16	$Co@SiO_2[(EtO)_3Si–L^3]/Co(II)$	Ethyl acetate	100	65
17	$Co@SiO_2[(EtO)_3Si–L^3]/Co(II)$	$CHCl_3$	100	69
18	$Co@SiO_2[(EtO)_3Si–L^3]/Co(II)$	Acetone	100	75
19	$Co@SiO_2[(EtO)_3Si–L^3]/Co(II)$	MeCN	100	84
20	$Co@SiO_2[(EtO)_3Si–L^3]/Co(II)$	CH_3OH	100	80

[a] Reaction condition: methyl phenyl sulfide (0.5 mmol), hydrogen peroxide 30% (90 μL, 0.881 mmol), catalyst 0.02 g, reaction time: 50 min, reaction temperature 55 °C.

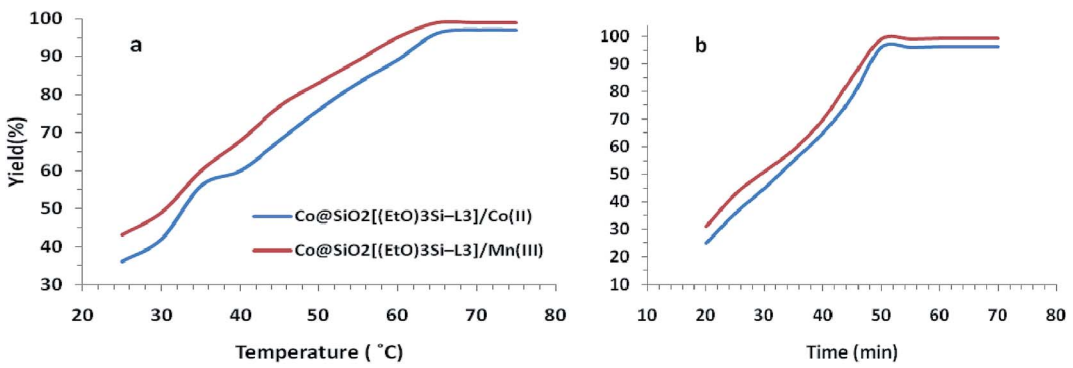

Fig. 8 Effect of temperature (a) and time (b) on the oxidation of methyl phenyl sulfide to methyl phenyl sulfoxide catalyzed by $Co@SiO_2[(EtO)_3Si–L^3]/Mn(III)$ (red) and $Co@SiO_2[(EtO)_3Si–L^3]/Co(II)$ (blue).

Table 2 The optimized amounts of the catalyst and oxidant in oxidation of methyl phenyl sulfide to methyl phenyl sulfoxide[a]

Entry	$Co@SiO_2[(EtO)_3Si–L^3]$/Mn(III) (g)	H_2O_2 30% (μL)	Selectivity (%)	Isolated yield
1	0.02	60	100	61
2	0.02	70	100	73
3	0.02	80	100	82
4	0.02	90	100	87
5	0.03	60	100	70
6	0.03	70	100	78
7	0.03	80	100	84
8	0.03	90	100	92
9	0.04	60	100	81
10	0.04	70	100	88
11	0.04	80	100	90
12	0.04	90	100	93
13	0.05	60	100	86
14	0.05	70	100	92
15	0.05	80	100	94
16	0.05	90	100	97
17	0.06	60	100	91
18	0.06	70	100	95
19	0.06	80	100	97
20	0.06	90	100	99
21	Not used	90	100	8

[a] Reaction condition: methyl phenyl sulfide (0.5 mmol), reaction time: 50 min, reaction temperature 65 °C.

a constant temperature of 65 °C and the reaction progress was monitored by TLC. Finally, the reaction time of 50 min was obtained as optimum time (Fig. 8b).

In addition to the solvent, time and temperature of the reaction, the other conditions such as catalyst amount and oxidant amount were investigated (Table 2). The amount of $Co@SiO_2[(EtO)_3Si–L^3]$/Mn(III) catalyst used in the reaction was varied in the range 0.02–0.06 (g). As shown in Table 2, increasing the amount of catalyst improved the yield and the maximum yield of the product was obtained with 0.06 g of catalyst. Also increasing the amount of H_2O_2 (30%), as an oxidizing agent, to 90 μL, increases the reaction yield (Table 2, entry 20).

To evaluate reusability of the catalyst, the oxidation of methyl phenyl sulfide was studied under optimum condition. After each cycle, the catalyst was separated by an external magnet, and washed several times with deionized water and ethanol. Then, it was dried in an oven at 50 °C and used in the next run. The results show that the synthesized catalysts can be reused seven times without any considerable loss in activity (Fig. 9).

Due to the relatively high magnetic capability of the present catalysts, it is easy to separate each of them by an external magnet. Moreover, due to the strong bond between functional groups with core and the presence of Schiff base groups, a strong bond with transition metals are formed in the complexes.

Performance capability of the catalyst $Co@SiO_2[(EtO)_3$-$Si–L^3]$/Mn(III) was evaluated by using different sulfides in

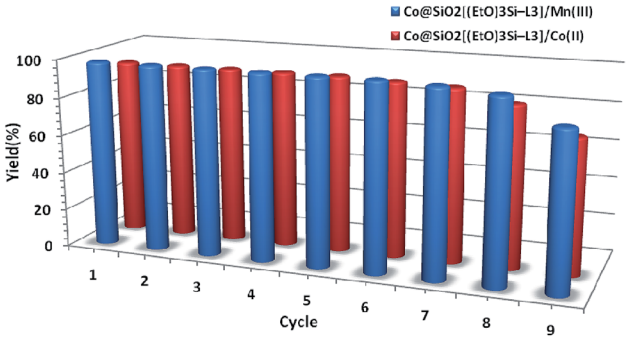

Fig. 9 Recycling of the two synthesized magnetic nanocatalysts used the oxidation of methyl phenyl sulfide to methyl phenyl sulfoxide.

oxidation reactions (Table 3). The results indicated that the catalyst is capable of oxidizing of sulfides with high yield.

Very recently some studies have been reported for sulfides oxidation using manganese(III) complexes.[17,22]

Therefore, the proposed mechanism for the performance of these complexes is shown in the Scheme 3.

Comparison with other catalysts

Comparative data on the performance of various catalysts in the oxidation of sulfides are shown in Table 4. Although Schiff base complexes are often used as efficient homogeneous catalysts for the oxidation reaction, some problems often exist in these types of oxidation studies, such as (1) deactivation, (2) instability and (3) expensive recycling of these homogeneous systems. Therefore, for improving the performance of catalytic activity, scientists tried to convert them into heterogeneous catalysts using a variety of methods. The greatest advantage of heterogeneous catalysis is the facile separation of catalysts from the reaction media and products. In order to fix catalysts onto heterogeneous supports, the different methods can be used, including grafting the catalyst onto inorganic supports such as silica. This is a very good method for synthesis of heterogeneous catalysts because of it eliminates some of the synthesis steps. However, a major challenge is the design of insoluble catalysts with high yields, selectivity, and cost effectiveness. According to all the above discussion, insoluble Schiff base complexes with good stability and catalytic activity are still rare and lack generality.

It is noteworthy that the reaction tolerates oxidation-sensitive functional groups and the sulfur atom is selectively oxidized. Synthetic processes for magnetic nanomaterials are currently undergoing rapid improvement and have opened up tremendous possibilities for the fabrication of magnetically-recoverable catalysts. Separation and recovery of catalysts by external magnetic field is an environmentally friendly alternative because not only does it minimize the use of auxiliary materials, but also prevents mass loss and reduces the operation time. We synthesized a highly active catalyst based on Schiff base complexes of Mn(III) or Co(II) ion supported on magnetic cobalt

Table 3 Oxidation of the variety of sulfides to sulfoxides by $Co@SiO_2[(EtO)_3Si–L^3]/Mn(III)$ nanocatalyst

Entry	Sulfides	Sulfoxides	Isolated yield (%)
1	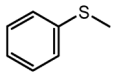	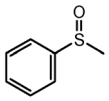	99
2	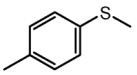	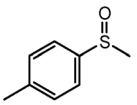	96
3	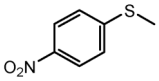	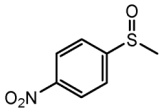	90
4	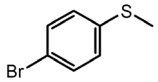	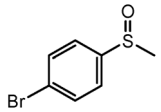	95
5	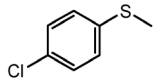	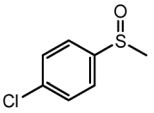	91
6	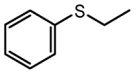	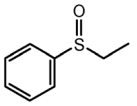	97
7	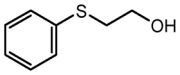	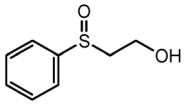	90
8	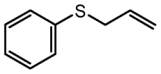	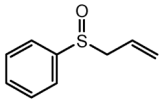	86
9	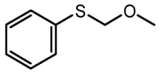	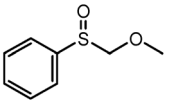	96
10	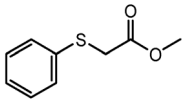	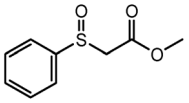	89
11	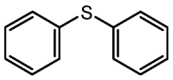	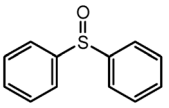	90
12	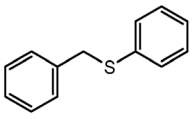	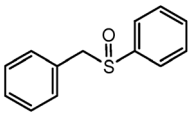	93
13	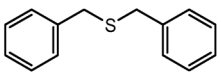	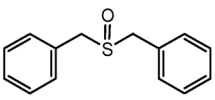	95

Table 3 (*Contd.*)

Entry	Sulfides	Sulfoxides	Isolated yield (%)
14	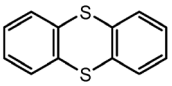	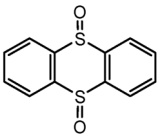	90
15	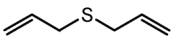	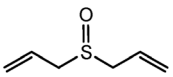	87
16	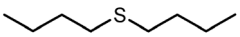	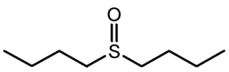	92
17			97

nanoparticles, which have been synthesized in a limited number in recent years. This synthesized catalysts were capable of catalyzing the oxidation reactions of alcohols[15] and sulfides with high yield. Further investigation of other catalytic reactions with this synthesized nanocatalyst is in progress. Other desirable properties of synthesized catalysts that are included in this publication are the high yield, short reaction time, selectivity, mild reaction conditions, and good catalyst recovery.

The efficiency of this method is demonstrated by comparing our results on the oxidation of benzyl phenyl sulfide with data from the literature. As shown in Table 4, the previously reported procedures suffer from one or more disadvantages such as longer reaction times,[31–36] low yield,[33–35] using a transition metal,[31–35] and the need for volatile and toxic organic solvents.[31–34,37]

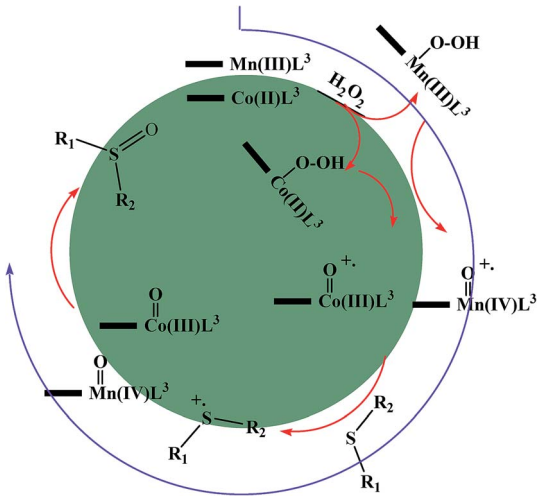

Scheme 3 Electron transfer mechanism for the $Co@SiO_2[(EtO)_3Si–L^3]/M$ (M = Mn(III) and Co(II)) catalyzed H_2O_2 oxidation of organic sulfides.

Table 4 Comparison of the activity of various catalysts in the oxidation of benzyl methyl sulfide using H_2O_2

Entry	Catalyst	Conditions	Time (min)	Yield (%)	Ref.
1	MNPs–PA	Solvent-free, rt	10	95	24
2	SSA	CH_3CN, rt	40	96	37
3	NBS	CH_3CN, 35–40 °C	15	90	36
4	Cu(II) complex, TEMPO	CH_3CN, 20 °C	20 h	52	33
5	$TaCl_5$	MeOH, 45 °C	150	96	34
6	$Cp/Mo(CO)_3Cl$	CH_3COCH_3–MeOH	330	92	31
7	Silica-based ammonium tungstate	CH_2Cl_2:MeOH, rt	240	83	32
8	$ZnBr_2$, pyridine-2-3-carboxylic acid	MeOH, rt	360	53	35
9	Schiff base/Cu(II) salen/Fe_3O_4	EtOH, 60 °C	180	83	23
10	$Co@SiO_2$@[Mn(III)SBC]	Solvent-free, 45 °C	40	92	24
11	Au/CTN-silica	60 °C	120	100	22
12	$Co@SiO_2[(EtO)_3Si–L^3]/Mn(III)$	55 °C	50	99	This work

Conclusion

In this study, the catalysts $Co@SiO_2[(EtO)_3Si–L^3]/Mn(III)$ and $Co@SiO_2[(EtO)_3Si–L^3]/Co(II)$ were successfully prepared *via* immobilizing the Schiff base ligand $[(EtO)_3Si–L^3H]$ on the Co nanoparticles coated with SiO_2 and then reacting them with metal salts *viz.* Mn(III) and Co(II). These catalysts were employed for the oxidation of the sulfides to sulfoxides and showed high catalytic activity and selectivity. It was further found that the catalyst can be easily isolated using an external magnet and reused seven times without significant catalytic deactivation.

These newly developed heterogeneous catalysts were simple to prepare. These catalysts were found to be easily reusable several times after reaction with an external magnet and drying without significant catalytic deactivation, which typically occurs due to the leaching of the active species or degradation of the structure. It appears that the Schiff base complex has played an important role in the stabilization of metal catalyst particles. These unique results open new perspectives for the application of these types of magnetic catalysts in other organic reactions.

Conflicts of interest

There are no conflicts to declare.

Acknowledgements

We thank the Payame Noor University, Bu-Ali Sina University and Center for Research and Development of Petroleum Technologies at Kermanshah, Research Institute of Petroleum Industry (RIPI), Iran for their partial support on this project.

References

1 M. V. Barmatova, I. D. Ivanchikova, O. A. Kholdeeva, A. N. Shmakov, V. I. Zaikovskii and M. S. Mel'gunov, *J. Mater. Chem.*, 2009, **19**, 7332.
2 A. K. Tucker-Schwartz and R. L. Garrell, *Chem.–Eur. J.*, 2010, **16**, 12718.
3 Y. Ma, B. Yue, L. Yu, X. Wang, Z. Hu, Y. Fan and Y. Chen, *J. Phys. Chem. C*, 2008, **112**, 472.
4 M. J. Jacinto, H. C. F. Santos, R. F. Jardim, R. Landers and L. M. Rossi, *Appl. Catal., A*, 2009, **360**, 177.
5 R. L. Oliveira, P. K. Kiyohara and L. M. Rossi, *Green Chem.*, 2010, **12**, 144.
6 L. Canali and D. C. Sherrington, *Chem. Soc. Rev.*, 1999, **28**, 85.
7 T. Katsuki, *Coord. Chem. Rev.*, 1995, **140**, 189.
8 R. Skoda-Foldes, L. Koll Jr and A. Arcadi, *J. Mol. Catal.*, 1995, **101**, 37.
9 B. S. Lane and K. Burgess, *Chem. Rev.*, 2003, **103**, 2457.
10 G. Righi and C. Bonini, *Synthesis*, 1994, **3**, 225.
11 G. X. Zheng, J. J. Eisch, Z. R. Lui and X. Ma, *J. Org. Chem.*, 1992, **57**, 5140.
12 L. P. C. Nielson, C. P. Stevenson, D. G. Backmond and E. N. Jacobsen, *J. Am. Chem. Soc.*, 2004, **126**, 1360.
13 J. Lopez, S. Liang and X. R. Bu, *Tetrahedron Lett.*, 1998, **39**, 4199.
14 A. M. Daly, C. T. Dalton, M. F. Renehan and D. G. Gilheany, *Tetrahedron Lett.*, 1999, **40**, 3617.
15 H. Keypour, S. G. Saremi, H. Veisi and R. Azadbakht, *RSC Adv.*, 2016, **6**, 77020.
16 M. Szavuly, S. D. Szilvasi, R. Csonka, D. Klesitz, G. Speier, M. Giorgi and J. Kaizer, *J. Mol. Catal. A: Chem.*, 2014, **393**, 317.
17 S. Rayati, F. Nejabat and S. Zakavi, *Inorg. Chem. Commun.*, 2014, **40**, 82.
18 P. Gogoi, M. Kalita, T. Bhattacharjee and P. Barman, *Tetrahedron Lett.*, 2014, **55**, 1028.
19 X. T. Zhou and H. B. Ji, *Catal. Commun.*, 2014, **53**, 29.
20 B. Yu, C. X. Guo, C. L. Zhong, Z. F. Diao and L. N. He, *Tetrahedron Lett.*, 2014, **55**, 1818.
21 Y. Imada, T. Kitagawa, S. Iwata, N. Komiya and T. Naota, *Tetrahedron*, 2014, **70**, 495.
22 A. R. Judy Azar, E. Safaei and S. Mohebbi, *Mater. Res. Bull.*, 2015, **70**, 753.
23 A. G. Choghamarani, Z. Darvishnejad and B. Tahmasbi, *Inorganica Chimica Acta*, 2015, **435**, 223.
24 A. Rostamia, B. Tahmasbia, F. Abedib and Z. Shokri, *J. Mol. Catal. A: Chem.*, 2013, **378**, 200.
25 F. Wang, C. Liu, G. Liu, W. Li and J. Liu, *Catal. Commun.*, 2015, **72**, 142.

26 M. Khorshidifard, H. A. Rudbari, B. Askari, M. Sahihi, M. R. Farsani, F. Jalilian and G. Bruno, *Polyhedron*, 2015, **95**, 1.
27 A. A. Manesh, F. H. Eshbal, S. Hemmatia and H. Veisi, *RSC Adv.*, 2015, **5**, 70265.
28 H. Veisi, F. H. Eshbal, S. Hemmatia and M. Baghayeri, *RSC Adv.*, 2015, **5**, 10152.
29 A. A. Manesh, F. H. Eshbala, S. Hemmatia and H. Veisi, *RSC Adv.*, 2015, **5**, 70265.
30 H. Keypour, M. Balalia, M. M. Haghdoost and M. Bagherzadeh, *RSC Adv.*, 2013, **00**, 1.
31 C. A. Gamelas, T. Lourenço, A. P. Costa, A. L. Simplício, B. Royo and C. C. Romão, *Tetrahedron Lett.*, 2008, **49**, 4708.
32 B. Karimi, M. Ghoreishi-Nezhad and J. H. Clark, *Org. Lett.*, 2005, **7**, 625.
33 S. Velusamy, V. A. Kumar, R. Saini and T. Punniyamurthy, *Tetrahedron Lett.*, 2005, **46**, 3819.
34 M. Kirihara, J. Yamamoto, T. Noguchi and Y. Hirai, *Tetrahedron Lett.*, 2009, **50**, 1180.
35 X. F. Wu, *Tetrahedron Lett.*, 2012, **53**, 4328.
36 B. Karimi and D. Zareyee, *J. Iran. Chem. Soc.*, 2008, **5**, 103.
37 A. Shaabani and A. H. Rezayan, *Catal. Commun.*, 2007, **8**, 1112.